Acta Crystallographica Section F
Structural Biology and Crystallization Communications
ISSN 1744-3091

Crystallization and preliminary X-ray analysis of immunophilin-like FKBP42 from *Arabidopsis thaliana*

Andreas Eckhoff,[a] Joachim Granzin,[a] Thilo Kamphausen,[b] Georg Büldt,[a] Burkhard Schulz[c,d] and Oliver H. Weiergräber[a]*

[a]Institut für Biologische Informationsverarbeitung (IBI-2, Biologische Strukturforschung), Forschungszentrum Jülich GmbH, D-52425 Jülich, Germany, [b]Max-Planck-Forschungsstelle für Enzymologie der Proteinfaltung, D-06120 Halle, Germany, [c]Universität Tübingen, ZMBP, D-72076 Tübingen, Germany, and [d]Purdue University, Department of Horticulture and Landscape Architecture, West Lafayette, IN 47907, USA

Correspondence e-mail: o.h.weiergraeber@fz-juelich.de

Received 20 January 2005
Accepted 28 February 2005
Online 12 March 2005

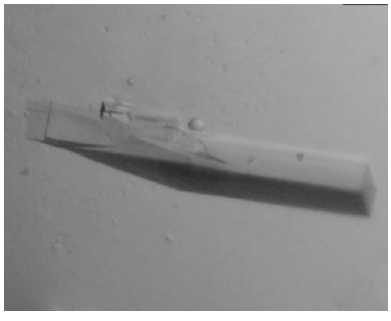

Two fragments of FKBP42 from *Arabidopsis thaliana* covering differing lengths of the molecule have been expressed, purified and crystallized. For each construct, crystals belonging to two different space groups were obtained and subjected to preliminary X-ray analysis.

1. Introduction

The FK506-binding proteins (FKBPs) represent an ancient and ubiquitous protein family named after the role of several members as primary targets of FK506-type immunosuppressants in animal and human cells (Galat, 2003). The FKBP–drug complex has been shown to block calcineurin (PP2B) mediated signal transduction, leading to an inhibition of the T-cell-dependent immune response (Cardenas *et al.*, 1999). This activity also led to the name 'immunophilins' for these proteins.

Another feature shared by many FKBPs is the ability to act as peptidylprolyl *cis–trans* isomerases (PPIases), which implicates these proteins in peptide-folding and chaperoning processes (Schiene & Fischer, 2000). Mammalian FKBP12, which comprises a single FKBP domain, has been shown to interact with different types of calcium-release channels (Jayaraman *et al.*, 1992; Cameron *et al.*, 1995) and to modulate their gating behaviour. Moreover, it associates with the type I receptors for TGFβ-family cytokines (Wang *et al.*, 1994), where it prevents ligand-independent activation. Multi-domain FKBPs are structurally characterized by additional protein modules, typically a tripartite tetratricopeptide repeat (TPR) domain and a calmodulin-binding motif, in addition to one or more FKBP domains. This group is exemplified by mammalian FKBP52, the major immunophilin of the multiprotein glucocorticoid receptor complex (Silverstein *et al.*, 1999). The crystal structure of human FKBP52 has been published recently (Wu *et al.*, 2004).

Members of the FKBP family have also been identified in plants. The crystal structure of *At*FKBP13, a single-domain FKBP localized in the thylakoid lumen of *Arabidopsis thaliana* chloroplasts, has been determined (Gopalan *et al.*, 2004). However, structural information on multi-domain FKBPs from plants is still unavailable.

*At*FKBP42, also termed Twisted Dwarf1 (TWD1) owing to the reduced height and disoriented growth of null mutants, contains a tripartite TPR motif, a calmodulin-binding site and a hydrophobic membrane anchor in addition to a single FKBP-type domain (Kamphausen *et al.*, 2002). The TPR region of *At*FKBP42 binds to *At*Hsp90, comparable to the complex formed by FKBP52 and Hsp90 in mammalian cells (Kamphausen *et al.*, 2002). Moreover, the FKBP domain of *At*FKBP42 has been demonstrated to physically interact with the nucleotide-binding domains of plasma membrane-localized ABC transporters *At*PGP1 and *At*PGP19 (Geisler *et al.*, 2003), whereas the TPR domain appears to be responsible for functional association with vacuolar transporters *At*MRP1 and *At*MRP2 (Geisler *et al.*, 2004).

It has been shown that the basipetal transport of the phytohormone auxin is required for establishment of plant polarity and development. Double mutants *atpgp1*/*atpgp19* display a subset of phenotypic features of *twd1*, which is accompanied by reduction of polar auxin transport (Geisler *et al.*, 2003). Therefore, it is tempting to

speculate that impaired cell elongation and disoriented growth of *twd1* plants may be caused by insufficient auxin transport.

The availability of an X-ray structure of *At*FKBP42 is expected to provide insight into the distinctive features of multi-domain plant FKBPs and to serve as a starting point for detailed investigations of the complexes with physiologically relevant target proteins, *e.g.* plant ABC transporters.

In this paper, we report the crystallization of two different fragments of *At*FKBP42 and present results from preliminary X-ray analysis using a synchrotron source.

2. Experimental procedures and results

2.1. Expression and purification

Initial experiments to express full-length *At*FKBP42 (residues 1–365) resulted in strong aggregation at a protein concentration of more than 2 mg ml^{-1}. The poor solubility may arise from the strong hydrophobic effect of the C-terminal membrane anchor. To overcome the problem, we proceeded with two N-terminal fragments of *At*FKBP42 comprising amino acids 1–180 and 1–339, respectively (Fig. 1). Both variants, hereafter named TWD$^{1–180}$ and TWD$^{1–339}$, could be concentrated to more than 40 mg ml^{-1}. Cloning, overexpression in *Escherichia coli* and purification have been described by Kamphausen *et al.* (2002). Briefly, transformed BL21 Codon+ RIL cells (Stratagene) were grown at 303 K and protein expression was induced with IPTG. Harvested cells were disrupted and a 100 000*g* supernatant was prepared. From this fraction, recombinant protein was purified by ion-exchange chromatography using a DEAE matrix and KCl as eluent. After pooling the relevant fractions, the material was dialyzed, passed over an AF-blue affinity column and concentrated. Final purification was performed by size-exclusion chromatography. The correct molecular mass and N-terminal sequence of the resulting protein were verified by mass spectrometry and automated N-terminal sequencing, respectively.

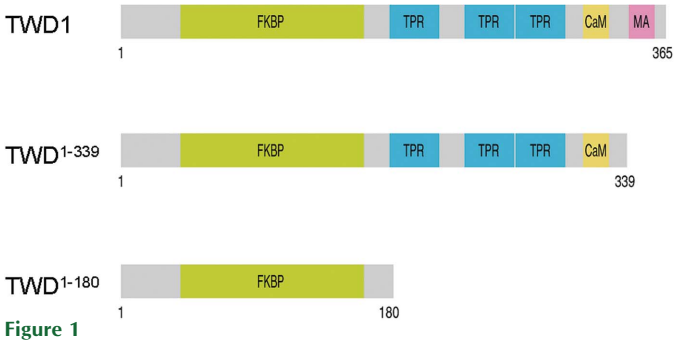

Figure 1
Predicted domain structure of full-length *At*FKBP42 (TWD1, top) and the truncated constructs (TWD$^{1–180}$ and TWD$^{1–339}$) described in this study.

2.2. Crystallization

The initial sparse-matrix screen for crystallization conditions of TWD$^{1–180}$ and TWD$^{1–339}$ was carried out using 98 different buffers from the Crystal Screen 1 and Crystal Screen 2 kits (Hampton Research). Both sitting-drop and hanging-drop vapour-diffusion methods were applied using 24-well plates sealed with cover slips and siliconized cover slips, respectively. Each sample was prepared by mixing 3 µl protein solution with an equal volume of reservoir buffer; the reservoir volume was 1 ml. All experiments were performed at T = 290 K. Crystals of TWD$^{1–180}$ could be detected after about 12 months in 2.5 *M* ammonium sulfate, 0.1 *M* NaCl, 0.1 *M* HEPES pH 8.0. Under optimized crystallization conditions, crystals could be obtained with 2.5 *M* ammonium sulfate, 0.1 *M* NaCl and 0.1 *M* Tris–HCl pH 8.0 using a protein concentration of 15 mg ml^{-1}. This condition simultaneously yielded two crystal forms, which will be referred to as type I (Fig. 2*a*) and type II (Fig. 2*b*), respectively.

TWD$^{1–339}$ crystals initially formed within about 10 months in 2.0 *M* ammonium sulfate, 2%(*v*/*v*) PEG 400 and 0.1 *M* HEPES pH 7.5. The improved conditions were 2.3 *M* ammonium sulfate, 2%(*v*/*v*) PEG 400 and 0.1 *M* HEPES pH 7.3–7.5 with a 28 mg ml^{-1} protein solution (type I; Fig. 2*c*). Independently, crystals were observed in 4 *M* sodium formate using a 40 mg ml^{-1} solution. Initially, a phase separation occurred with formation of droplets. Between 3 and 12 months a reduction of the the droplets was accompanied by the appearance of protein crystals with a convex surface (type II; Fig. 2*d*), possibly indicating a transformation of the liquid protein phase into solid crystals.

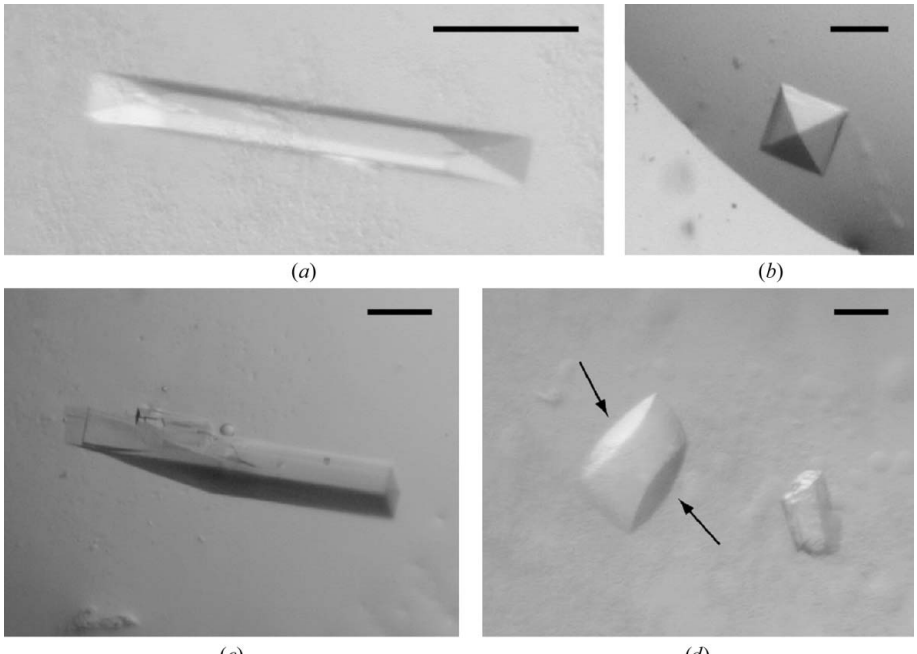

Figure 2
Representative photographs showing the different crystal forms observed for TWD$^{1–180}$ (*a*, *b*) and TWD$^{1–339}$ (*c*, *d*). TWD$^{1–180}$ type I (*a*) and TWD$^{1–339}$ type I (*c*) crystals display a prismatic habit. TWD$^{1–339}$ type II (*d*) crystals present an irregular set of surfaces, in part with convex curvature (arrows), whereas TWD$^{1–180}$ type II (*b*) forms tetragonal bipyramids. Scale bars indicate 100 µm.

2.3. X-ray data collection and analysis

Crystallographic data sets were collected at T = 100 K. The crystals were step-soaked in reservoir solution containing 5–30%(*v*/*v*) glycerol prior to cryocooling.

Native data sets for type I crystals of TWD$^{1–180}$ as well as type I and II crystals of TWD$^{1–339}$ were recorded at beamline ID14-1 of the ESRF (Grenoble, France) tuned to a wavelength of λ = 0.934 Å on an ADSC Q4R detector (ADSC Quantum). Data collection for type II crystals of TWD$^{1–180}$ was performed at beamline

Table 1
X-ray crystallographic data.

Values for the highest resolution shells are indicated in parentheses.

	TWD$^{1-180}$		TWD$^{1-339}$	
	Type I	Type II	Type I	Type II
Space group	$P2_12_12_1$	$P4_222$	$P2_12_12$	$C222_1$
Unit-cell parameters (T = 100 K)				
a (Å)	35.0	122.6	86.1	68.8
b (Å)	62.8	122.6	117.9	123.0
c (Å)	122.8	151.0	40.1	87.2
Resolution (Å)	2.3 (2.30–2.42)	3.1 (3.10–3.18)	2.9 (2.90–3.06)	2.3 (2.30–2.36)
ESRF beamline	ID14-1	ID14-3	ID14-1	ID14-1
Detector	ADSC Q4R	MAR CCD	ADSC Q4R	ADSC Q4R
Wavelength (Å)	0.934	0.931	0.934	0.934
Observed reflections	178062	261580	112876	117766
Unique reflections	12298	21551	9584	16798
Average multiplicity	6.2	4.5	3.5	3.8
Completeness (%)	97.1 (98.2)	92.5 (76.1)	98.5 (97.4)	99.8 (99.6)
$R_{\rm meas}$† (%)	6.0 (25.4)	13.3 (41.3)	5.4 (42.2)	4.6 (25.4)
$\langle I/\sigma(I)\rangle$	8.6 (3.2)	4.7 (2.2)	12.5 (2.1)	8.0 (3.4)
Molecules per AU	1–2	4–8	1	1
Solvent content (%)	26–63	30–65	53	48

† $R_{\rm meas} = \sum_h [N_h/(N_h-1)]^{1/2} \sum_i |I_{i,h} - \langle I_h\rangle| / \sum_h \sum_i I_{i,h}$, with $I_{i,h}$ representing the ith of N_h measurements and $\langle I_h\rangle$ the mean of all observations of I_h (Diederichs & Karplus, 1997).

ID14-3 (λ = 0.931 Å) on a MAR CCD detector (MAR Research). All native crystals diffracted to resolutions ranging from 3.1 to 2.3 Å. Data processing and scaling were carried out using *MOSFLM* (Leslie, 1992) and *SCALA*, part of the *CCP*4 program suite (Collaborative Computational Project, Number 4, 1994). For detailed data statistics refer to Table 1.

The larger fragment of *At*FKBP42 crystallizes in orthorhombic space groups, $P2_12_12$ for type I and $C222_1$ for type II, whereas for the shorter construct we found $P2_12_12_1$ for crystals of type I and $P4_222$ for type II. Despite apparent similarities in unit-cell parameters, analysis for metric relationships using *TRACER* (Collaborative Computational Project, Number 4, 1994) and *LEPAGE* (Spek, 1988) did not reveal any valid cell transformation for either space-group pair. The occurrence of two different space groups for TWD$^{1-180}$ is remarkable since the respective crystals appeared under the same conditions and even in the same droplet. This may indicate a case of true polymorphism. However, it cannot be excluded that the two crystal types arose from slightly different molecular species, possibly resulting from proteolytic processing. The latter may in principle also be true for TWD$^{1-339}$, although in this case the fundamentally different crystallization conditions provide a convincing explanation for the finding of different space groups. SDS–PAGE analysis of the mother liquor from representative experiments revealed broadening of protein bands, corresponding to a narrow spectrum of molecular weights. While this finding could be interpreted in terms of an exopeptidase activity acting on the termini, we hope to confirm the exact size of the crystallized molecules during structure determination.

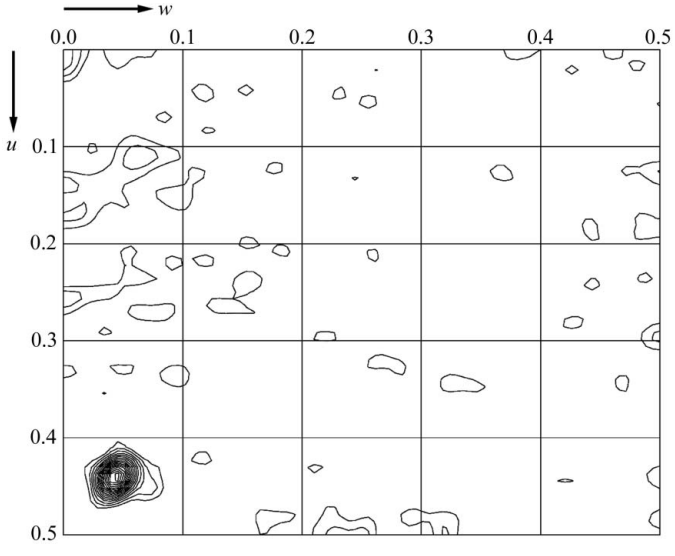

Figure 3
Native Patterson map (section v = 0.5) of a TWD$^{1-180}$ type II data set showing the 17.5σ translation peak at u = 0.44, w = 0.04. The map is contoured in 1σ steps.

Preliminary information concerning the packing of NCS-related monomers in the asymmetric unit of the tetragonal TWD$^{1-180}$ crystals were obtained using self-rotation functions (*POLARRFN*; Collaborative Computational Project, Number 4, 1994) as well as native Patterson maps. The self-rotation map does not reveal any significant peaks apart from those expected from the crystallographic symmetry (point group 422) at polar coordinates ω = 0, κ = 90° as well as at ω = 90, φ = 0/φ = 45, κ = 180°. This implies that the non-crystallographic axes, if present, are probably oriented roughly parallel to the crystallographic axes. The native Patterson map (Fig. 3), on the other hand, displays a 17.5σ translation peak at u = 0.44, v = 0.5, w = 0.04 which is 8% of the height of the origin peak. Based on these observations, we speculate that the asymmetric unit may be composed of two dimers or two tetramers.

For determination of protein structures, we are planning to apply molecular replacement with search models derived from the X-ray structures of human FKBP12 (PDB code 1fkf) for the FKBP-like domain and bovine cyclophilin 40 (PDB code 1ihg) for the TPR domain, with at least 30% sequence identity in either case.

We thank the beamline scientists at the ESRF (Grenoble, France), where the data sets were recorded.

References

Cameron, A. M., Steiner, J. P., Sabatini, D. M., Kaplin, A. I., Walenski, L. D. & Snyder, S. H. (1995). *Proc. Natl Acad. Sci. USA*, **92**, 1784–1788.
Cardenas, M. E., Cruz, M. C., Del Poeta, M., Chung, N., Perfect, J. R. & Heitman, J. (1999). *Clin. Microbiol. Rev.* **12**, 583–611.
Collaborative Computational Project, Number 4 (1994). *Acta Cryst.* D**50**, 760–763.
Diederichs, K. & Karplus, P. A. (1997). *Nature Struct. Biol.* **4**, 269–275.
Galat, A. (2003). *Curr. Top. Med. Chem.* **3**, 1315–1347.
Geisler, M., Girin, M., Brandt, S., Vincenzetti, V., Plaza, S., Paris, N., Kobae, Y., Maeshima, M., Billion, K., Kolukisaoglu, Ü. H., Schulz, B. & Martinoia, E. (2004). *Mol. Biol. Cell*, **15**, 3393–3405.
Geisler, M., Kolukisaoglu, H. Ü., Bouchard, R., Billion, K., Berger, J., Saal, B., Frangne, N., Koncz-Kalman, Z., Koncz, C., Dudler, R., Blakeslee, J. J., Murphy, A. S., Martinoia, E. & Schulz, B. (2003). *Mol. Biol. Cell*, **14**, 4238–4249.
Gopalan, G., He, Z., Balmer, Y., Romano, P., Gupta, R., Heroux, A., Buchanan, B. B., Swaminathan, K. & Luan, S. (2004). *Proc. Natl Acad. Sci. USA*, **101**, 13945–13950.
Jayaraman, T., Brillantes, A., Timerman, A. P., Fleischer, S., Erdjument-Bromage, H., Tempst, P. & Marks, A. R. (1992). *J. Biol. Chem.* **267**, 9474–9477.
Kamphausen, T., Fanghänel, J., Neumann, D., Schulz, B. & Rahfeld, J.-U. (2002). *Plant J.* **32**, 263–276.
Leslie, A. G. W. (1992). *Jnt CCP4/ESF–EACBM Newsl. Protein Crystallogr.* **26**.
Schiene, C. & Fischer, G. (2000). *Curr. Opin. Struct. Biol.* **10**, 40–45.
Silverstein, A. M., Galigniana, M. D., Kanelakis, K. C., Radanyi, C., Renoir, J. M. & Pratt, W. B. (1999). *J. Biol. Chem.* **274**, 36980–36986.
Spek, A. L. (1988). *J. Appl. Cryst.* **21**, 578–579.
Wang, T., Donahoe, P. K. & Zervos, A. S. (1994). *Science*, **265**, 674–676.
Wu, B., Li, P., Liu, Y., Lou, Z., Ding, Y., Shu, C., Ye, S., Bartlam, M., Shen, B. & Rao, Z. (2004). *Proc. Natl Acad. Sci. USA*, **101**, 8348–8353.